Quantifying Mass Transport during Polarization in a Li Ion Battery Electrolyte by in Situ ^{7}Li NMR Imaging

Matilda Klett,[†] Marianne Giesecke,[‡] Andreas Nyman,[†] Fredrik Hallberg,[‡] Rakel Wreland Lindström,[†] Göran Lindbergh,[†] and István Furó*[,‡]

[†]Division of Applied Electrochemistry, Department of Chemical Engineering and Technology, and [‡]Division of Applied Physical Chemistry, Department of Chemistry, KTH Royal Institute of Technology, SE-10044 Stockholm, Sweden

S *Supporting Information*

ABSTRACT: Poor mass transport in the electrolyte of Li ion batteries causes large performance losses in high-power applications such as vehicles, and the determination of transport properties under or near operating conditions is therefore important. We demonstrate that in situ ^{7}Li NMR imaging in a battery electrolyte can directly capture the concentration gradients that arise when current is applied. From these, the salt diffusivity and Li^{+} transport number are obtained within an electrochemical transport model. Because of the temporal, spatial, and chemical resolution it can provide, NMR imaging will be a versatile tool for evaluating electrochemical systems and methods.

Limited mobility of ions in the electrolyte has a great negative effect on the performance of Li ion batteries in high-power applications. Irreversible losses related to the limited mobility are manifested in a voltage drop comprising both ohmic polarization and polarization from concentration gradients in the electrolyte, which build up as a result of mass-transport limitations and are dependent on the electrolyte composition and operating conditions of the battery. It is therefore of great importance to understand and quantify the electrolyte properties that define the battery performance during operation, including the conductivity, diffusivities, and transport numbers[1]. The conductivity characterizes the electrolyte in the absence of concentration gradients. The diffusivities and transport numbers, where the latter denote the fraction of current carried by certain species, describe the mass transport and formation of concentration gradients. All three parameters should be included in an evaluation of an electrolyte to predict its behavior during battery operation.

Diffusivities and transport numbers of battery electrolytes can be measured spectroscopically using, for example, diffusion NMR[2−4] or electrophoretic NMR (eNMR) spectroscopy,[5−7] the latter method being more suitable for nondilute electrolytes. The transport parameters can also be obtained electrochemically through a series of polarization/relaxation experiments, concentration cell experiments, and impedance measurements.[8,9] Electrochemical methods probe the mass transport indirectly by measuring the potential at the current collectors and correlating it to the salt concentration. Local salt concentrations are estimated via electrochemical models. Alternatively, a direct measurement of the salt concentration across a battery cell would enable a rapid assessment of the mass transport and mass transport parameters under load and would also be useful for validating and developing electrochemical models.

In-situ measurements of the spatial distribution of lithium ions in batteries are scarce and rely on, for example, in situ Raman spectrometry,[10,11] optical imaging,[12,13] and most recently neutron imaging (radiography).[14] The need for access and transparency severely limits optical methods. In-situ NMR experiments have previously been shown to be valuable in monitoring structural changes in battery electrodes during charge/discharge.[15−21] However, NMR imaging that can determine spatial distributions has only rarely been applied to batteries.[15,22] Chandrashekar et al.[22] recently demonstrated the use of NMR imaging to characterize lithium dendrite formation in a symmetric lithium/lithium cell upon application of a current.

Here we report the use of in situ one-dimensional (1D) ^{7}Li NMR imaging to obtain temporally and spatially resolved concentration profiles in a LiPF$_6$ electrolyte while applying a constant current. From the gradual buildup of concentration gradients in a cell, the diffusion coefficient and Li^{+} transport number are extracted using a concentrated binary electrolyte mass transport model.[9]

The measurements were performed in a home-built cell fitted inside a 10 mm NMR tube. This cell was developed on the basis of a previous cell[23] used for measuring electro-osmotic transport in fuel cell membranes. The cell design (Figure 1A) allows a confined electrolyte column to be held between two lithium metal electrodes (100 μm foils) connected to external wires for in situ current control. The electrolyte of study was 1 M LiPF$_6$ in 1:1 ethylene carbonate (EC)/diethylene carbonate (DEC) mixed with 15 wt % poly(methyl methacrylate) (PMMA). The NMR imaging experiments were always performed starting from sample cells newly assembled under an argon atmosphere. Electrochemical impedance spectroscopy (EIS) was performed on each sample cell after assembly to ensure reproducibility. During in situ polarization using a current of 30−50 μA, 1D NMR images with a 17 min acquisition time were collected every 33 min for 14−18 h.

The results presented here were recorded with the current direction setting the cathode on top. The images were recorded using spin−echo experiments with the magnetic field gradient applied along the z direction (see Figure 1A). The echo time

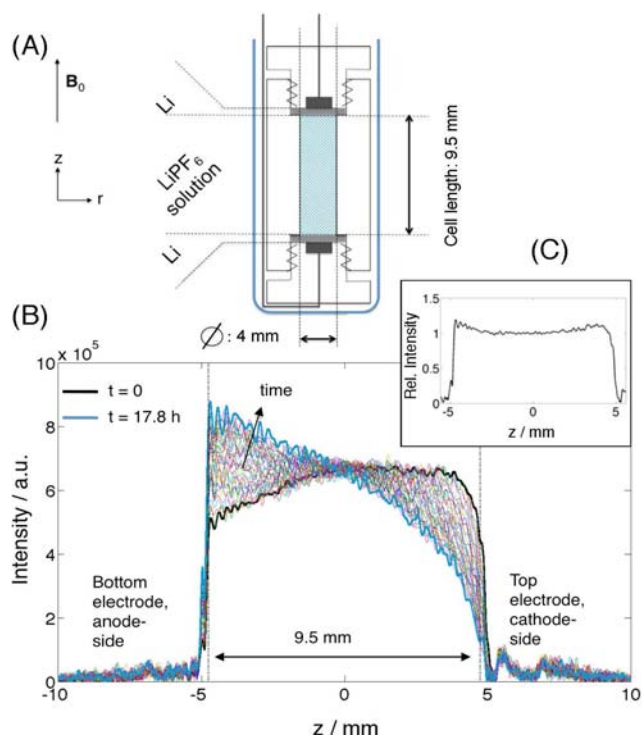**Figure 1.** (A) Schematic picture of the electrochemical cell. (B) 1D ^{7}Li NMR images taken over the cell, to which a constant current of 30 μA was applied. Two of the images are highlighted: one before the current was applied ($t = 0$; black curve) and the other after application of the current for $t = 17.8$ h (blue curve). (C) Concentration profile at $t = 0$ normalized to the RF sensitivity profile (see the text) used to account for the inhomogeneity of the radiofrequency field.

was set sufficiently long to suppress the signal from any metallic lithium,[24] and the image acquisition time was chosen as a compromise between signal/noise ratio and time resolution. The currents applied were selected to cause substantial concentration gradients but to stay below limiting currents during the entire experimental time. See the Supporting Information (SI) for electrolyte properties and the experimental setup.

Figure 1B displays 34 images obtained during the application of a current of 30 μA for 17.8 h. The development of concentration gradients over time is clearly visible. The sharp image edges define the electrolyte column. The nominal resolution was 19 μm. One would expect a flat Li profile at $t = 0$, but there was a clear deviation from that, caused by the varying radiofrequency field (RF) strength and sensitivity[25] along the z direction. As detailed in the SI, this latter effect could be quantified by measuring an RF sensitivity profile. Normalizing the obtained raw image at $t = 0$ to this profile recovered the expected rectangular shape (Figure 1C). The slight deviations at the edges are due to susceptibility effects at the metal−electrolyte interface.

By the application of different currents, the system was shown to respond as expected: the higher the current, the greater the concentration difference across the cell (Figure 2). Here the images were normalized to the corresponding sample cell profile at $t = 0$, which was measured before the current was applied with 2048 scans in order to reduce noise. While in general the setup was robust and reproducible, deviations between profiles with identical currents were sometimes observed close to the cell edges (e.g., samples 3 and 4 in
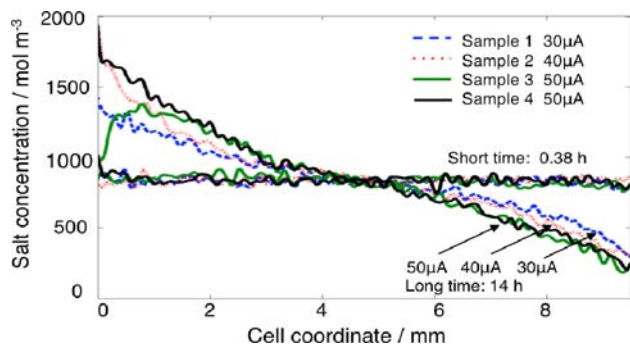

Figure 2. NMR profiles normalized to the corresponding $t = 0$ profile for four samples with constant applied currents of (sample 1) 30, (sample 2) 40, and (samples 3 and 4) 50 μA at times $t = 0.38$ and 14 h.

Figure 2). This seemed to be caused by accidental deformation of the corresponding soft Li metal electrode plate during assembly of the cell.

Although the electrolyte used here exhibited high viscosity (recall the added PMMA), convection could still appear in the cell. First, when the current direction is such that the salt concentration becomes high at the top, one should obtain increasing mass density at the top of the cell. Indeed, when current was applied in that configuration, we found no consistent buildup of concentration gradients, which showed that convective flow must have occurred. Hence, all of the experiments reported here were performed using the current direction leading to higher concentration and thus a higher mass density at the cell bottom (Figure 1B). Convection might still arise because of Joule heating, which in a cylindrical cell would lead to a warmer center. This effect could be excluded because of the low average power (estimated as ca. 5×10^{-5} W with a voltage drop of <1 V over the cell) and because we obtained consistent transport parameters with different currents and thus different heating. The heating effect from the imaging gradients was also estimated to be negligible (on the order of 0.1 K or less). ^{1}H NMR diffusion experiments performed with different diffusion times[26] indicated that, if present, any convection proceeded with an average flow velocity of <10^{-3} mm/s (see the SI for more details).

With the obtained temporally and spatially resolved Li$^+$ concentration profiles, $c_+(z, t)$, the transport parameters can be evaluated by solving a partial differential equation describing the mass transport and fitting the solution, $c_{+,calc}(z, t, p)$, where p represents the fitting parameters, to the experimental data. A number of different models can be formulated, depending on the electrolyte studied and the desired level of complexity. We used a previously reported mass transport model[9] describing a concentrated electrolyte consisting of a binary salt and a single solvent (an approximation for the EC/DEC/PMMA mixture). The model takes into account solvent transport due to the movement of the salt by expressing the solvent flux in terms of the anion flux and the salt and solvent molar volumes, denoted as V_m^s and V_m^0, respectively. The local Li$^+$ concentration can thus be obtained by solving the continuity equation for the anion PF$_6^-$; since $c_- = c_+ = c_s$, this equation can be expressed as

$$\frac{\partial c_s}{\partial t} = \frac{\partial}{\partial z}\left\{(1 - c_s V_m^s)\left[\left(1 + \frac{\partial \ln f}{\partial \ln c_s}\right)\frac{c_{tot}}{c_0}D\frac{\partial c_s}{\partial z}\right.\right.$$
$$\left.\left. + \frac{i(1 - t_+^0)}{F}\right]\right\} \tag{1}$$

with the boundary condition of zero anion flux at the electrode surfaces and a uniform initial concentration of c_{s0}. Here the indices +, −, 0, and s denote the cation, anion, solvent, and salt, respectively; $D = 2D_{+0}D_{-0}/(D_{+0} + D_{-0})$ is the salt diffusion coefficient with respect to the thermodynamic driving force, expressed in terms of the Maxwell−Stefan diffusivities D_{+0} and D_{-0}; f is the activity coefficient of the salt; i is the current density; t_+^0 is the cation transport number with respect to the solvent mixture; F is the Faraday constant; and $c_0 = (1 - V_m^s c_s)/V_m^0$ and $c_{tot} = 2c_s + c_0$ are the solvent and total concentrations, respectively.

The parameters t_+^0 and $D_{s,TF} = D[1 + (\partial \ln f/\partial \ln c_s)]$, the latter of which includes both D and the thermodynamic factor in eq 1, were obtained in the data fitting and assumed to be independent of concentration. The quality of the fits is illustrated in Figure 3, which presents data obtained at a
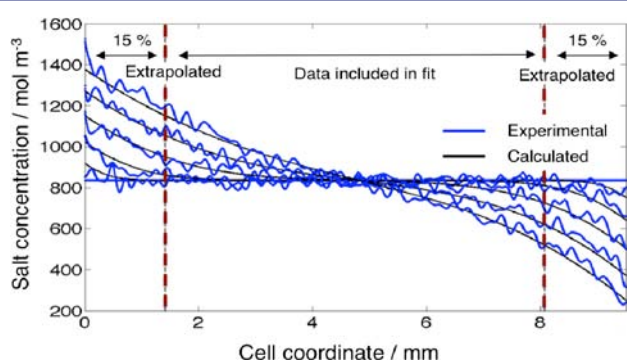

Figure 3. Experimental (normalized to $t = 0$ data) and fitted salt concentrations obtained for a sample using a current of 30 μA applied for 0.4, 2.0, 5.8, 11.3, and 17.8 h.

current of 30 μA (for clarity, only six images are displayed, but all of the images for any given current were included in the fitting procedure). To suppress errors arising from the irreproducible edge effects discussed earlier, we fitted data only from the interior of the electrolyte column, and data close to the edges were cut off, as shown in Figure 3. In most cases, extrapolated data in the cutoff regions showed good agreement with the experimental points there. Data obtained by cutting off 15% of the cell length on each side are shown in Table 1. Data obtained by cutting off 10% of the cell length were also tested and provided a ca. 5% change in the parameters t_+^0 and $D_{s,TF}$ (see the SI). The concentration profiles were approximated as instantaneous images obtained at the midpoint of the 17 min acquisition window. The largest error from neglecting the time averaging during the image accumulation should appear at the edges and at short times, where the concentration changed most rapidly. We found, however, that the error introduced from neglecting the time averaging was sufficiently small to allow for the approximation (see the SI).

In Table 1, the average values of the fitting parameters obtained at different currents are shown with the customarily defined standard deviation. We also derived the apparent diffusion coefficient, $D_{s,app}$, and the transport number with

Table 1. Definitions, Average Values, and Sample Standard Deviations (σ) of the Obtained Transport Parameters

parameter	definition	average	σ
$D_{s,TF}$	$D[1 + (\partial \ln f/\partial \ln c_s)]$	9.6[a]	1.9[a]
$D_{s,app}$	$D_{s,TF}(c_{tot}/c_0)(1 - c_s V_m^s)$	11[a]	2.1[a]
t_+^0	$D_{+0}/(D_{+0} + D_{-0})$	0.20	0.035
t_+^{room}	$1 - t_-^0(1 - c_s V_m^s)$	0.24	0.033
D_+	cation self-diffusion	3.8[a,b]	–
D_-	anion self-diffusion	7.72[a,b]	–
t_+	$D_+/(D_+ + D_-)$	0.33[b]	–

[a]Units: 10^{-11} m^2/s. [b]Obtained from diffusion NMR measurements.

respect to the room, t_+^{room}, which reflects the current ratio carried by the cation defined in the fixed coordinate system of the electrochemical cell (in contrast to t_+^0, which is defined relative to the moving solvent). For comparison, the ion-specific self-diffusion coefficients, D_+ and D_-, and the derived Li$^+$ transport number, t_+, obtained by diffusion NMR measurements are also listed (see the SI).

The transport numbers have been reported to be typically less than 0.4 for Li$^+$ in liquid electrolytes commonly used in Li ion batteries at the present time.[3,4,9,27,28] The low transport number obtained here, $t_+^{room} = 0.24$, shows that only a small fraction of the current is carried by Li$^+$. Since current is also carried by the nonreacting PF$_6^-$ ions, a concentration gradient develops. The parameters obtained here are in good overall agreement with those obtained for similar systems. Nyman et al.[9] reported $t_+^{room} = 0.3$ and $D_{s,app} = 4 \times 10^{-10}$ m^2/s for 0.8 M LiPF$_6$ in an EC/ethyl methyl carbonate mixture in an electrochemical study using the same model as employed here. Zugmann et al.[28] reported $t_+^{room} = 0.24$ for 1 mol kg^{-1} LiPF$_6$ in EC/DEC using the galvanostatic polarization method, which was developed for nonideal solid electrolytes.[8]

From Table 1, it can also be seen that t_+ is larger than the transport number obtained by NMR imaging analysis. A similar discrepancy between a larger transport number obtained from diffusion NMR analysis relative to that from eNMR measurements[7] and electrochemical measurements has been reported previously[4,7,28] and can be partly explained by the fact that the definition of t_+ given in Table 1 is valid only for dilute electrolytes. The values of transport parameters are inherently dependent on the formulation and assumptions of the model. In a pragmatic light, it is advantageous to obtain parameters defined in the same frame of reference as in the application where they are to be used (e.g., in electrochemical models predicting performance).[29−33] Direct measurements of concentration, as presented here, allow for validation of models used in the electrochemical community. In particular, this could be useful for studies of complex electrolytes with multicomponent transport.[34]

As discussed above, we evaluated the data under the assumption that the parameters are independent of concentration. In the future, the concentration dependence of the parameters could be explicitly taken into account by performing experiments with different starting concentrations and allowing for a self-consistent polynomial variation of the parameters with concentration in the fit. The time resolution was sufficient for data evaluation at the currents applied here (see the SI) but could be further optimized. For example, in the systems investigated here, one could reduce the image acquisition time to 10 s by changing the nucleus from lithium to fluorine (currently not allowed because of the use of Teflon as the cell

material); this would permit investigations of smaller and more realistic cells at higher currents and/or with complex current schemes. Ultimately, one could approach a real battery regarding, for example, geometry[22] and components.

In conclusion, we have reported the application of NMR imaging for direct visualization of the buildup of concentration gradients in a battery electrolyte under load. We have demonstrated the use of the technique to quantify the diffusivity and the transport number on the basis of a physical mass transport model. The data analysis using this method is very flexible regarding the model description and parameter fitting. Measuring the concentration with spatial and temporal resolution allows this noninvasive spectroscopic technique to be used both as a fast method to detect concentration polarization and to validate transport parameters obtained by nondirect electrochemical methods. We envisage that NMR imaging will become a useful tool for investigating a range of electrochemical systems that shall further our understanding of electrolyte behavior in real applications and support the development of novel battery systems.

■ ASSOCIATED CONTENT

Ⓢ Supporting Information
Cell assembly, electrolyte characteristics, NMR experiments, and data evaluation. This material is available free of charge via the Internet at http://pubs.acs.org.

■ AUTHOR INFORMATION

Corresponding Author
furo@kth.se

Notes
The authors declare no competing financial interest.

■ ACKNOWLEDGMENTS

■ REFERENCES

(1) Newman, S. J. *Electrochemical Systems*, 2nd ed.; Prentice Hall: Englewood Cliffs, NJ, 1991.

(2) Saito, Y.; Yamamoto, H.; Nakamura, O.; Kageyama, H.; Ishikawa, H.; Miyoshi, T.; Matsuoka, M. *J. Power Sources* **1999**, *81*, 772.

(3) Capiglia, C.; Saito, Y.; Kageyama, H.; Mustarelli, P.; Iwamoto, T.; Tabushi, T.; Tukamoto, H. *J. Power Sources* **1999**, *81*, 859.

(4) Zhao, J.; Wang, L.; He, X.; Wan, C.; Jiang, C. *J. Electrochem. Soc.* **2008**, *155*, A292.

(5) Dai, H.; Zawodzinski, T. A. *J. Electrochem. Soc.* **1996**, *143*, L107.

(6) Walls, H. J.; Zawodzinski, T. A. *Electrochem. Solid-State Lett.* **2000**, *3*, 321.

(7) Walls, H. J.; Fedkiw, P. S.; Zawodzinski, T. A.; Khan, S. A. *J. Electrochem. Soc.* **2003**, *150*, E165.

(8) Ma, Y. P.; Doyle, M.; Fuller, T. F.; Doeff, M. M.; Dejonghe, L. C.; Newman, J. *J. Electrochem. Soc.* **1995**, *142*, 1859.

(9) Nyman, A.; Behm, M.; Lindbergh, G. *Electrochim. Acta* **2008**, *53*, 6356.

(10) Rey, I.; Bruneel, J. L.; Grondin, J.; Servant, L.; Lassègues, J. C. *J. Electrochem. Soc.* **1998**, *145*, 3034.

(11) Georen, P.; Adebahr, J.; Jacobsson, P.; Lindbergh, G. *J. Electrochem. Soc.* **2002**, *149*, A1015.

(12) Brissot, C.; Rosso, M.; Chazalviel, J. N.; Lascaud, S. *J. Electrochem. Soc.* **1999**, *146*, 4393.

(13) Harris, S. J.; Timmons, A.; Baker, D. R.; Monroe, C. *Chem. Phys. Lett.* **2010**, *485*, 265.

(14) Siegel, J. B.; Lin, X.; Stefanopoulou, A. G.; Hussey, D. S.; Jacobson, D. L.; Gorsich, D. *J. Electrochem. Soc.* **2011**, *158*, A523.

(15) Gerald, R. E.; Klinger, R. J.; Sandi, G.; Johnson, C. S.; Scanlon, L. G.; Rathke, J. W. *J. Power Sources* **2000**, *89*, 237.

(16) Gerald, R. E.; Sanchez, J.; Johnson, C. S.; Klinger, R. J.; Rathke, J. W. *J. Phys.: Condens. Matter* **2001**, *13*, 8269.

(17) Chevallier, F.; Letellier, M.; Morcrette, M.; Tarascon, J.-M.; Frackowiak, E.; Rouzaud, J.-N.; Béguin, F. *Electrochem. Solid-State Lett.* **2003**, *6*, A225.

(18) Letellier, M.; Chevallier, F.; Morcrette, M. *Carbon* **2007**, *45*, 1025.

(19) Letellier, M.; Chevallier, F.; Clinard, C.; Frackowiak, E.; Rouzaud, J.-N.; Béguin, F.; Morcrette, M.; Tarascon, J.-M. *J. Chem. Phys.* **2003**, *118*, 6038.

(20) Key, B.; Bhattacharryya, R.; Morcrette, M.; Seznec, V.; Tarascon, J.-M.; Grey, C. P. *J. Am. Chem. Soc.* **2009**, *131*, 9239.

(21) Bhattacharryya, R.; Key, B.; Chen, H.; Best, A. S.; Hollenkamp, A. F.; Grey, C. P. *Nat. Mater.* **2010**, *9*, 504.

(22) Chandrashekar, S.; Trease, N. M.; Chang, H. J.; Du, L.-S.; Grey, C. P.; Jerschow, A. *Nat. Mater.* **2012**, *11*, 311.

(23) Hallberg, F.; Vernersson, T.; Pettersson, E. T.; Dvinskikh, S. V.; Lindbergh, G.; Furó, I. *Electrochim. Acta* **2010**, *55*, 3542.

(24) Holcomb, D. F.; Norberg, R. E. *Phys. Rev.* **1955**, *98*, 1074.

(25) Hoult, D. I. *Prog. Nucl. Magn. Reson. Spectrosc.* **1978**, *12*, 41.

(26) Hedin, N.; Yu, T. Y.; Furó, I. *Langmuir* **2000**, *16*, 7548.

(27) Valoen, L. O.; Reimers, J. N. *J. Electrochem. Soc.* **2005**, *152*, A882.

(28) Zugmann, S.; Fleischmann, M.; Amereller, M.; Gschwind, R. M.; Wiemhöfer, H. D.; Gores, H. *J. Electrochim. Acta* **2011**, *56*, 3926.

(29) Nyman, A.; Zavalis, T. G.; Elger, R.; Behm, M.; Lindbergh, G. *J. Electrochem. Soc.* **2010**, *157*, A1236.

(30) Fuller, T. F.; Doyle, M.; Newman, J. *J. Electrochem. Soc.* **1994**, *141*, 1.

(31) Arora, P.; Doyle, M.; Gozdz, A. S.; White, R. E.; Newman, J. *J. Power Sources* **2000**, *88*, 219.

(32) Mellgren, N.; Brown, S.; Vynnycky, M.; Lindbergh, G. *J. Electrochem. Soc.* **2008**, *155*, A304.

(33) Albertus, P.; Christensen, J.; Newman, J. *J. Electrochem. Soc.* **2009**, *156*, A606.

(34) Nyman, A.; Behm, M.; Lindbergh, G. *J. Electrochem. Soc.* **2011**, *158*, A628.